Engineering Structures 141 (2017) 373–385

Contents lists available at ScienceDirect

Engineering Structures

journal homepage: www.elsevier.com/locate/engstruct

Analytical study on reinforced concrete frames subject to compressive arch action

Shao-Bo Kang [a,b,*], Kang Hai Tan [c]

[a] Key Laboratory of New Technology for Construction of Cities in Mountain Area (Chongqing University), Ministry of Education, Chongqing 400045, China
[b] School of Civil Engineering, Chongqing University, Chongqing 400045, China
[c] School of Civil and Environmental Engineering, Nanyang Technological University, Singapore 639798, Singapore

ARTICLE INFO

Article history:
Received 29 October 2015
Revised 13 March 2017
Accepted 20 March 2017

Keywords:
Compressive arch action
Analytical model
Column stiffness
Joint shear
Column flexural resistance

ABSTRACT

Reinforced concrete beams can resist applied vertical loads through the development of compressive arch action (CAA) when adequate horizontal restraints are provided at the ends. However, at the frame level, CAA tends to push adjoining columns outwards and may induce premature flexural or shear failure to the columns. Therefore, under CAA, flexural and shear resistances of the connecting columns need to be examined. This paper describes an analytical study on the behaviour of reinforced concrete frames subject to CAA. In the study, lateral and rotational stiffness of reinforced concrete columns is determined based on a rigid-plastic assumption. CAA of reinforced concrete frames is investigated through an analytical model, in which deformations of columns are taken into consideration. Besides, shear force and bending moment in the column are calculated from equilibrium to shed light on the possible failure mode of columns under CAA. Parametric studies are also conducted to investigate the dominant parameters on the behaviour of columns. Finally, recommendations are provided for the design of reinforced concrete columns against CAA in the connecting beam.

1. Introduction

When restrained against horizontal movements, reinforced concrete beams and slabs can develop significant net axial compression force and arch action between compression zones, which in turn enhances the load resistance of beams and slabs. Park proposed a rigid-plastic model for estimating the compressive arch action (CAA) of reinforced concrete slabs [1]. It was assumed in the model that tensile reinforcement has yielded and compressive concrete attains its ultimate strain. Besides, flexural deformations of the beam are concentrated at the plastic hinges at the beam ends, whereas the beam segment itself remains rigid. Thereafter, shortening of the beam induced by axial compression force was introduced to the model [2,3]. The effects of imperfect boundary conditions, such as rotation of supports and connection gaps in horizontal restraints, were also incorporated in the model by Guice et al. [4] and Yu and Tan [5]. The rigid-plastic model was further extended to the elastic stage of the deformed beam by determining the strain profile across the beam end sections according to compatibility [6], in which strain-hardening behaviour of high-performance fibre-reinforced concrete was taken into consideration as well. To date, the effects of axial and rotational restraints, beam span-depth ratio and reinforcement ratio on the CAA of beams have been well investigated [5]. Furthermore, pseudo-static resistance of beams was calculated based on the energy-balance method proposed by Izzudin et al. [7]. It was concluded that development of CAA increases the quasi-static load capacity but reduces the ductility of beams, thereby enhancing the pseudo-static resistance marginally [6].

However, focus of previous analytical studies was primarily placed on the CAA of reinforced concrete beams with fairly rigid boundary conditions, in which stocky column stubs with sufficient flexural and shear resistances were provided at the ends of beams [8–13]. Limited effort was made to evaluate the behaviour of comparatively slender columns when subject to CAA in the adjoining beams. Experimental results of reinforced concrete frames demonstrate that columns may exhibit shear failure as a result of additional shear force in the beam-column joints [14–16]. Therefore, it is imperative to assess the resistances of side columns and beam-column joints under CAA in the connecting beams.

This paper presents an analytical study on the behaviour of reinforced concrete frames with realistic columns adjoining to bridging beams. An analytical model for CAA of reinforced concrete frames is introduced. In the model, the compatibility condition for bridging beams developed by Yu and Tan [5] is adopted in the study. To determine the strains and forces in steel reinforcement

* Corresponding author at: School of Civil Engineering, Chongqing University, Chongqing 400045, China.
E-mail address: skang2@e.ntu.edu.sg (S.-B. Kang).

http://dx.doi.org/10.1016/j.engstruct.2017.03.039
0141-0296/

and concrete, the method proposed by Kang and Tan [6] is utilised, and lateral and rotational stiffness of columns is considered. A rigid-plastic model is also derived to determine the stiffness of reinforced concrete columns. The analytical model for CAA is validated against experimental results of Kang and Tan [14,17], Yu [18] and Sadek et al. [15] and reasonably good agreement is achieved. Finally, parametric studies are conducted to investigate the dominant parameters on potential flexural and shear failure of columns. Special attention is paid to the shear force in beam-column joints and bending moment acting on columns, endeavouring to gain insight into the potential failure mode of columns subject to CAA in adjacent beams.

2. Analytical model for compressive arch action

For an exterior reinforced concrete frame, which comprises of a bridging beam, a middle joint and two side columns and is simply-supported at the inflection points of the columns, development of CAA is accompanied by net axial compression force in the beam. Due to insufficient lateral and rotational stiffness of the columns, side beam-column joints are pushed outwards by a horizontal displacement of t as a result of beam axial compression force. Meanwhile, hogging moment at the side joint face generates a rigid-body rotation of Θ in the side joints. Fig. 1 shows the deformed geometry of the frame. Thus, in deriving the analytical model for CAA, deflection of the column and rotation of the joint need to be considered.

2.1. Compatibility condition

Due to symmetry, the single-span beam, middle and side joints are isolated from the prototype frame. Fig. 2 shows the compatibility condition of the beam. The horizontal distance between points A and B can be determined from the movement and rotation of the support as well as the deformed geometry of the beam, as expressed in Eq. (1). Accordingly, vertical displacement δ at the middle joint can be calculated from Eq. (2).

$$l + 0.5\varepsilon_b h_c + t - 0.5h\tan\Theta = (l(1-\varepsilon_b) + (h-c_1)\tan(\varphi-\Theta) - c_2\tan\varphi)\cos\varphi \quad (1)$$

$$\delta = (l + 0.5\varepsilon_b h_c + t - 0.5h\tan\Theta)\tan\varphi \quad (2)$$

where l is the clear span of the beam; ε_b is the axial compressive strain of the beam; h_c and h are the depths of the column and the beam, respectively; t is the horizontal movement of the side joint caused by beam axial force; c_1 and c_2 are the neutral axis depths at And 12; φ is the rotation of the beam; Θ is the rotation of the side joint; and δ is the vertical displacement of the middle joint.

Besides the whole beam, compatibility at Sections 1 and 2 has also to be satisfied. It is assumed that the strain of top longitudinal reinforcement is zero at the inflection point of the beam and varies linearly along the beam length, as shown in Fig. 2. Correspondingly, deformations of top reinforcement at Sections 1 and 2 can be determined from the summation of steel strains between the inflection point and end sections, as expressed in Eqs. (3) and (4). Lengths of beam segments l_1 and l_2 can be quantified from bending moments at Sections 1 and 2.

$$\Delta l_1 = (h - c_1 - a_{s1})\tan(\varphi - \Theta) = 0.5\varepsilon_{s1} l_1 \quad (3)$$

$$\Delta l_2 = (c_2 - a'_{s2})\tan\varphi = 0.5\varepsilon'_{s2} l_2 \quad (4)$$

where a_{s1} is the spacing between the extreme tension fibre of the beam and the centroid of tensile reinforcement at Section 1; a'_{s2} is the spacing between the extreme compression fibre of the beam and the centroid of compressive reinforcement at Section 2; ε_{s1} and ε'_{s2} are the respective strains of reinforcement at Sections 1 and 2; and l_1 and l_2 are the distances between the inflection point of the beam and Sections 1 and 2, respectively.

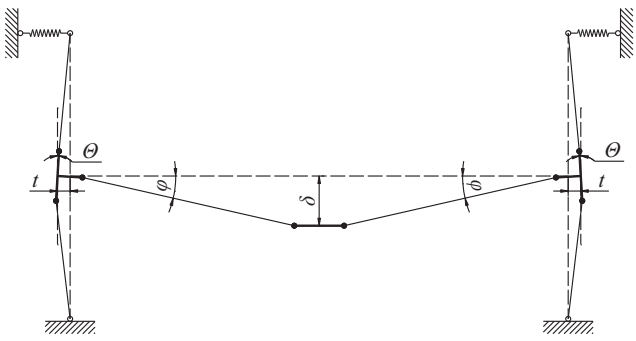

Fig. 1. Deformed geometry of a reinforced concrete frame.

2.2. Equilibrium condition

Besides compatibility, equilibrium of the deformed beam can be established from the free-body diagram, as shown in Fig. 3. At a vertical displacement δ of the middle joint, vertical load P on the middle joint is equilibrated by bending moments M_1 and M_2, beam compression force N and self-weight q of the beam. Eq. (5) expresses the equilibrium of the beam. Net axial compression force in the beam is correlated to its axial strain via Eq. (6).

$$P = \frac{2(M_1 + M_2 - N\delta - ql^2/2)}{l} \quad (5)$$

$$N = bhE_c\varepsilon_b \quad (6)$$

where M_1 and M_2 are the bending moments at Sections 1 and 2, calculated from internal forces (see Fig. 2); N is the beam axial compression force; q is the self-weight of the beam; P is the vertical load on the middle joint; b is the beam width; and E_c is the elastic modulus of concrete.

2.3. Constitutive models for concrete and steel reinforcement

To determine the forces sustained by concrete and steel reinforcement, constitutive models for concrete and reinforcing bars have to be defined. Previous analytical studies assumed that extreme compression concrete fibre attains its ultimate strain and equivalent rectangular concrete stress block was used to calculate the compression force [1,5,19]. However, it leads to substantial overestimation of vertical load before the CAA capacity is attained. To accurately predict the ascending branch of the vertical load, stress-strain model for concrete proposed by Mander et al. [20] is utilised in the analytical model instead of equivalent compressive stress block. Compression force in concrete is calculated through integration of compressive stress across the compression zone. Similar approach is also used to compute the contribution of concrete compression force to bending moment. Besides, a bilinear stress-strain relationship is employed for tensile steel reinforcement. For compressive reinforcing bars, a linear unloading branch is defined, with its stiffness identical to the elastic modulus of steel reinforcement.

2.4. Solution procedures

Prior to analysis, material and geometric properties and boundary conditions of reinforced concrete frames need to be determined. With compatibility, equilibrium and constitutive models

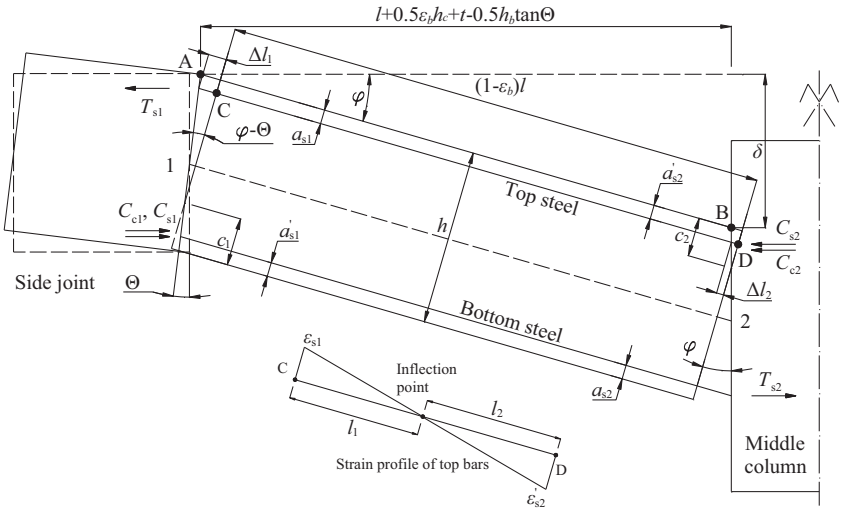

Fig. 2. Compatibility of reinforced concrete beam.

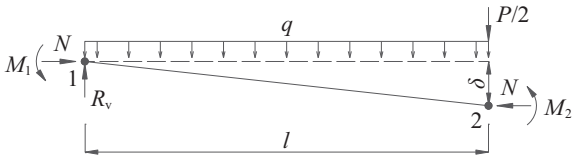

Fig. 3. Equilibrium condition of single-span beam.

for concrete and steel reinforcement, a set of solution procedures is proposed for the analytical model as follows.

Step 1: Provide a rotation φ of beam and calculate l_1 and l_2 from bending moments at Sections 1 and 2 that are determined from previous step. For the first step, it can be assumed that l_1 is equal to l_2.
Step 2: Assume a neutral axis depth c_1 at Section 1.
Step 3: Assume a bending moment M_1 at Section 1 and calculate rotation Θ of the side joint; thereafter, compute strain ε_{s1} of the tensile reinforcement from Eq. (3). Strain profile at Section 1 is determined based on plane-section assumption. Correspondingly, net axial force and bending moment M_1 can be calculated. Once the calculated bending moment is equal to the assumed value, equilibrium at Section 1 is satisfied.
Step 4: Assume a neutral axis depth c_2 at Section 2 and determine strain ε'_{s2} of the compressive reinforcement from Eq. (4). Similarly, strain profile, axial compression force and bending moment at Section 2 can be quantified. If net axial forces at Sections 1 and 2 are equal to one another, equilibrium of the beam is satisfied.
Step 5: Calculate axial strain ε_b of the beam from Eq. (6); thereafter, check the compatibility of the beam through Eq. (1). When it is satisfied, vertical load P and associated displacement δ can be determined from Eqs. (5) and (2), respectively.

3. Determination of column stiffness

As a prerequisite of the analytical model for CAA, lateral and rotational stiffness of reinforced concrete columns needs to be determined experimentally or analytically. In experimental tests, the stiffness of columns can be quantified from the lateral load-displacement relationship and bending moment-rotation relationship of columns. When axial compression force in the beam and bending moment at the beam end cannot be obtained from experimental results, analytical study is necessary to evaluate the stiffness of columns. In this study, the rigid-plastic assumption is also used for determining the lateral and rotational stiffness of columns.

3.1. Rigid-plastic model for column

It is assumed that a beam-column joint is located at the mid-height of a simply-supported column, namely, l_t is equal to l_b, as shown in Fig. 4. Besides, the beam-column joint remains rigid and flexural deformations of the column are concentrated at the column-joint interfaces. When subject to a point load P at the beam-column joint, the column develops a horizontal deflection of δ_c at the joint and the extreme concrete fibre is compressed by Δl_c (see Fig. 4(a)). From compatibility of the column, Δl_c can be computed from neutral axis depth c at the joint face, as expressed in Eq. (7).

$$\Delta l_c = c\tan\theta_c = c\tan\left(\frac{\delta_c}{l_t}\right) \tag{7}$$

where c is the neutral axis depth at the joint interface; θ_c is the rotation of the column segment relative to the joint; δ_c is the lateral displacement at the column-joint interface; and l_t is the length of the column segment above the joint.

Under a bending moment M_c, the joint experiences a rigid body rotation of θ_r, as shown in Fig. 4(b). Horizontal deflection of the column at the joint face can be determined as:

$$\delta_c = \frac{1}{2}h\sin\theta_r \tag{8}$$

where θ_r is the rotation of the joint.

Thus, rotation θ_c of the column section relative to the joint face is calculated from Eq. (9).

$$\theta_c = \frac{\delta_c}{l_t} + \frac{2\delta_c}{h} \tag{9}$$

In calculating the strain ε_c of extreme compression concrete fibre, a linear strain profile is assumed between the pin support and the joint face, as shown in Fig. 4(a and b). Correspondingly, Δl_c and ε_c are correlated through Eq. (10). Thereafter, strain profile at the column-joint interface can be determined from the plane-section assumption.

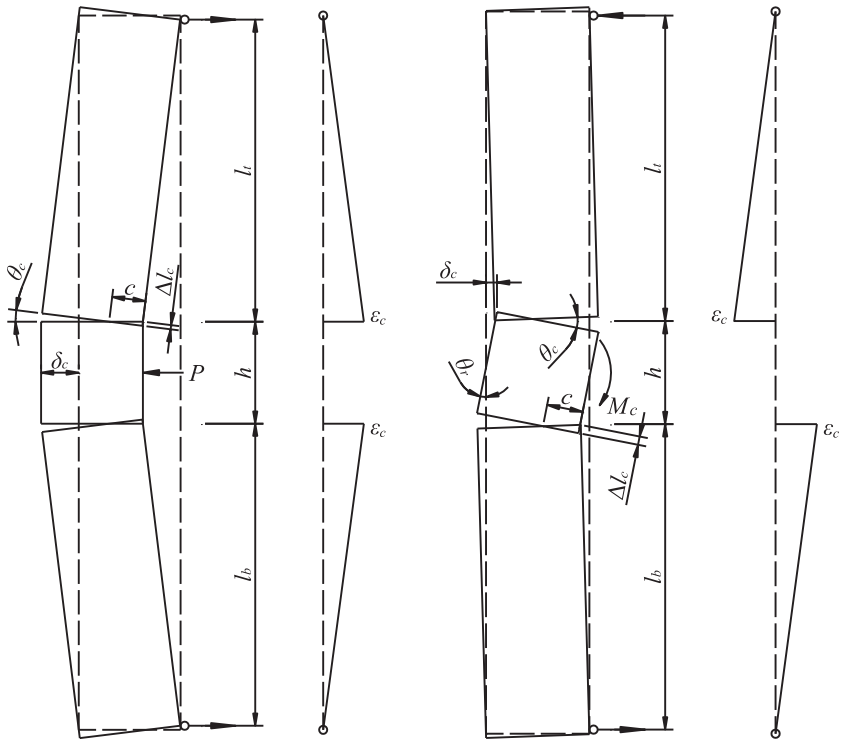

Fig. 4. Rigid-plastic model for reinforced concrete column.

$$\Delta l_c = \frac{l_t \varepsilon_c}{2} \tag{10}$$

where ε_c is the strain of extreme compression concrete fibre at the joint face.

Forces sustained by steel reinforcement and concrete can be calculated from the strains and associated stress-strain models. Other than equivalent rectangular concrete stress block, compression force carried by concrete is determined by integrating the concrete stress across the compression zone. When the calculated axial force in the column is equal to the applied value, bending moment at the joint face can be quantified. Accordingly, horizontal force or bending moment acting on the joint can be calculated in accordance with the force equilibrium of the column.

3.2. Verification of rigid-plastic model

To evaluate the accuracy of the rigid-plastic model, four reinforced concrete columns tested by Soesianawati [21] and Watson and Park [22] are simulated through the model. Table 1 summarises the material and geometric properties of the columns. In the tests, the height and cross section of the columns were kept constant. Compression forces with axial load ratios ranging from 0.1 to 0.3 were applied to the columns. Load capacities of the columns are calculated through the analytical model, as included in Table 1. The average ratio of the analytical to experimental peak loads is 0.95, indicating that the rigid-plastic model yields reasonably good predictions of the load capacity of reinforced concrete columns. Furthermore, envelope curves of load-displacement response can also be obtained through the model, as shown in Fig. 5. The analytical load-displacement curves are in good agreement with the experimental results.

As different axial load ratios were used for reinforced concrete column units 1 and 2, lateral load-displacement curves of the columns are greatly different from one another, as shown in Figs. 5(a and b). Thus, it is necessary to evaluate the effect of axial compression force on the load-displacement relationship of columns. Fig. 6 shows the lateral load-displacement curves of unit 4, with a range of axial load ratios from 0.1 to 0.3. With increasing axial compression force, the column develops greater initial stiffness and higher load capacity. However, the ductility is reduced as a result of crushing of concrete in the compression zone. A further increase in the axial load ratio may result in crushing of compressive concrete prior to yielding of tensile reinforcement. Therefore, the rigid-plastic model for columns is capable of simulating the effect of axial compression force on the load-displacement curve of the column.

3.3. Prediction of column stiffness

Lateral and rotational stiffness of reinforced concrete columns can be calculated based on the rigid-plastic model. Experimental and analytical results suggest that the stiffness of columns decreases gradually with increasing lateral load and bending moment prior to attaining the load capacity. In this study, the secant stiffness of columns corresponding to yielding of tensile reinforcement is used. Besides, experimental values of the column stiffness are also quantified from the lateral load-deflection and bending moment-joint rotation curves. Table 2 shows the comparisons between analytical and experimental stiffness of precast concrete frames tested by Kang and Tan [14,17]. It is noteworthy that an axial load ratio of 0.3 was used for all columns. Generally, lateral and rotational stiffness of the columns is overestimated by around 25% through the rigid-plastic model. It is possibly due to the existence of concrete interface between precast concrete column and cast-in-situ joint which reduced the stiffness of columns.

Besides the stiffness of reinforced concrete columns, effective moment of inertia can also be determined from the model, as included in Table 3. When columns with an axial load ratio of 0.3

Table 1
Comparison between analytical and experimental load capacities.

Columns	Column height (mm)	Column section (mm)	Concrete strength (MPa)	Axial force ratio γ_a	Rebar	m	Peak load (kN)		
							Cal.	Exp.	Cal./Exp.
Unit 1	3600	400 × 400	47	0.1	12T16	446	388	402	0.96
Unit 2			44	0.3			530	562	0.94
Unit 3			44				531	560	0.95
Unit 4			40				501	523	0.96

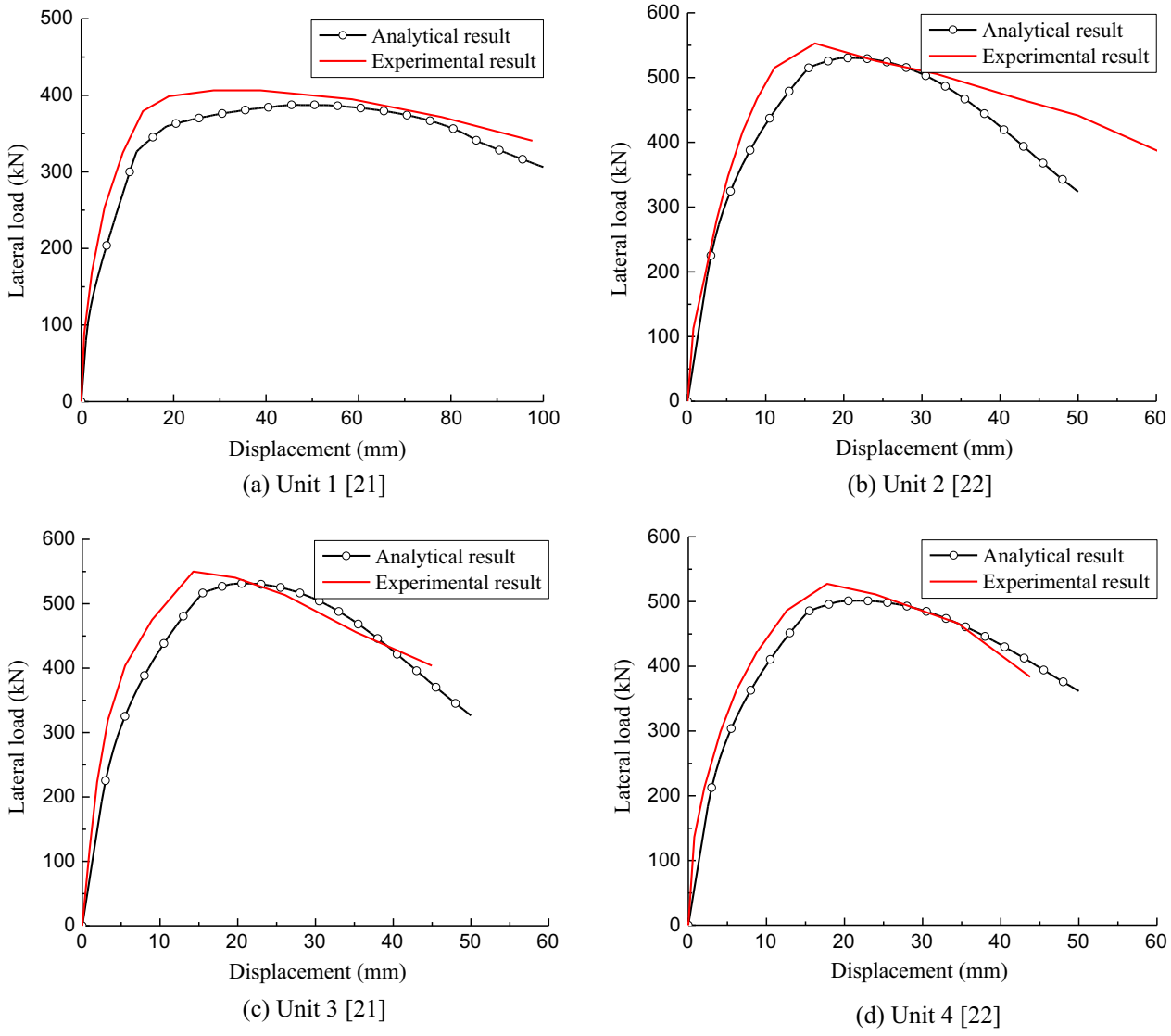

Fig. 5. Lateral load-displacement curves of reinforced concrete columns (the lateral load and displacement can be determined from Eqs. (7) and (10), respectively).

are subject to bending moment at the joint, the effective moment of inertia calculated from the rigid-plastic model agrees well with that recommended by ACI [23] and Paulay and Priestley [24]. However, under lateral load, the value is around 30% smaller than the recommended ones. Hence, utilisation of the recommended effective moment of inertia results in an overestimation of the lateral stiffness of columns.

4. Estimation of compressive arch action

CAA of precast concrete frames is estimated through the analytical model. Fig. 7 shows the vertical load-displacement curves of frames tested by Kang and Tan [14,17]. Column stiffness calculated from experimental tests is used in the model. The analytical results agree well with the experimental ones prior to fracture of bottom steel reinforcement at the joint interface. However, strains of tensile reinforcement at the beam ends are underestimated due to the linear assumption of strain profile between the inflection point and end sections of the beams. As a result, rupture of reinforcement cannot be simulated in the model. Axial compression force in the beam can also be predicted by the model, as shown in Fig. 8. At the initial stage, beam axial force is underestimated significantly before cracking of the column, as the stiffness of the column used in the model is much less than that of the uncracked column. After cracking of the column, the analytical axial force-displacement

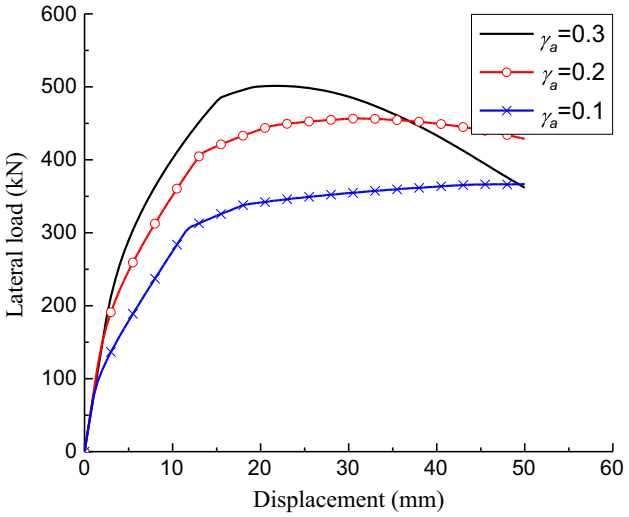

Fig. 6. Effect of axial load on lateral load-displacement relationship of Unit 4.

curves are in good agreement with experimental results. However, due to premature diagonal shear cracking of side beam-column joints, vertical displacement associated with the maximum axial compression is overestimated in frames EF-B-0.88-0.59 and EF-B.

Reinforced concrete frames reported by Yu [18] and Sadek et al. [15] are also simulated by the model. As limited information on the stiffness of columns is available, the rigid-plastic model for columns is used to estimate the lateral and rotational stiffness of the columns. Table 4 summarises the CAA capacity and maximum axial force in the beam. Beam axial forces in IMF and SMF were not measured in the tests, and thus only analytical results are included. Comparisons between analytical and experimental results indicate that the analytical model is capable of predicting the CAA capacity of frames with reasonably good accuracy. The average ratio of analytical to experimental CAA capacities is 0.99, with a coefficient of variation of 4%. Compared to the experimental result, the analytical axial compression is slightly overestimated, with an average ratio of 1.02 and a coefficient of variation of 15%. However, for IMF and SMF, the maximum axial compression forces in the beam are substantially greater than the numerical values provided by Lew et al. [25], possibly as a result of neglecting the slippage of column footing in the analytical model.

5. Parametric studies

Through the analytical model, the effects of column height, column section and beam depth on the CAA and axial compression force in the beam are investigated. Besides, shear force and bending moment in the side beam-column joint are evaluated based on equilibrium of the column. Frame EF-B-S tested by Kang and Tan [14] is selected as the control specimen. Table 5 summarises the geometry and stiffness of reinforced concrete columns. In the parametric studies, the lateral and rotational stiffness of columns is calculated through the rigid-plastic model for columns.

5.1. Effect on vertical load and beam axial force

Fig. 9 shows the vertical load-displacement curves and beam axial force-displacement curves of reinforced concrete frames with various column heights. It is notable that negative values of the axial force represent compression. By shortening the column height from 3.34 m to 1.34 m, CAA capacity of the frame is increased by 27% (see Fig. 9(a)). Likewise, axial compression force in the beam is increased from 47.6 kN to 267.8 kN, as shown in Fig. 9(b). However, vertical displacements associated with the CAA capacity and peak compression force are reduced. The increases in the vertical load and beam axial force derive from higher lateral and rotational stiffness provided by a shorter column. When the column height is reduced from 3.34 m to 1.34 m, lateral and rotational stiffness of the column is increased by 25 and 2.5 times, respectively, as included in Table 5.

Similar results can be obtained in the analytical model by enlarging the cross section of the column, as shown in Fig. 10. When the column section is 250 mm square, approximately the same flexural action and CAA capacities, 73.8 kN and 75.4 kN, respectively, are obtained for the frame, even though axial compression force of 71.6 kN develops in the beam. Increasing the cross section of the square column from 250 mm to 400 mm leads to an increase of CAA capacity by 23% from 75.4 kN to 92.7 kN, whereas the flexural action capacity of the frame remains nearly identical (see Fig. 10(a)). Meanwhile, the net compression force in the beam is increased by 125.9 kN from 71.6 kN to 198.5 kN, as shown in Fig. 10(b). Nonetheless, vertical displacements associated with the CAA capacity and maximum compression force are reduced due to greater lateral and rotational stiffness of the column with larger cross section. Thus, reducing the column height or increasing the cross section is beneficial to the development of CAA in the adjacent beam.

Furthermore, the effect of beam depth on the CAA of the beam is investigated analytically. For a given longitudinal reinforcement ratio, reinforced concrete beams with greater depth are capable of developing higher sagging and hogging moment capacities, and the flexural action capacity is increased, as shown in Fig. 11(a). Besides, lateral and rotational stiffness of the columns with identical height is slightly increased by an increase in beam depth (see Table 5). Fig. 11 shows the effect of beam depth on the CAA capacity and maximum compression force in the beam. As beam depth increases, both CAA capacity and axial compression force in the beam are increased. Compared to that of 250 mm depth (with CAA capacity of 59.9 kN), the CAA capacity of the 400 mm deep beam is increased by around 119% to 130.9 kN and vertical

Table 2
Stiffness of reinforced concrete columns.

Specimen		Column height (m)	Column section (mm)	Rebar	Lateral stiffness (kN/m)			Rotational stiffness (kN.m/rad)		
					Cal.	Exp.	Cal./ Exp.	Cal.	Exp.	Cal./ Exp.
Kang and Tan [17]	EF-B-0.88-0.59	2.34	250 × 250	8T13	1.17×10^4	8.8×10^3	1.33	1.36×10^4	7.7×10^3	1.77
	EF-L-0.88-0.59					9.5×10^3	1.23		8.3×10^3	1.64
Kang and Tan [14]	EF-B					9.0×10^3	1.3		1.44×10^4	0.94
	EF-L					1.12×10^4	1.04		1.56×10^4	0.87
	EF-B-S		300 × 300		2.28×10^4	1.75×10^4	1.30	2.72×10^4	2.51×10^4	1.08
	EF-L-S					2.02×10^4	1.13		2.28×10^4	1.19
Mean value							1.22			1.25
Coefficient of variation							9%			30%

Table 3
Effective moment of inertia of columns.

Effective moment of inertia		Column under lateral load	bending momentColumn under
Rigid-plastic model	250 × 250	$0.49I_g$	$0.64I_g$
	300 × 300	$0.46I_g$	$0.67I_g$
ACI [23]		$0.70I_g$	
Paulay and Priestley [24]		$0.67I_g$	

displacement corresponding to the CAA capacity is also larger, as shown in Fig. 11(a). It is noteworthy that the enhancement of CAA to flexural action is also substantially increased. Additionally, the beam develops 138.1 kN greater axial compression force by enlarging the beam depth to 400 mm. However, associated vertical displacement does not vary significantly (see Fig. 11(b)). Analytical results indicate that increasing the beam depth is also an effective way to mobilise greater CAA in the beam.

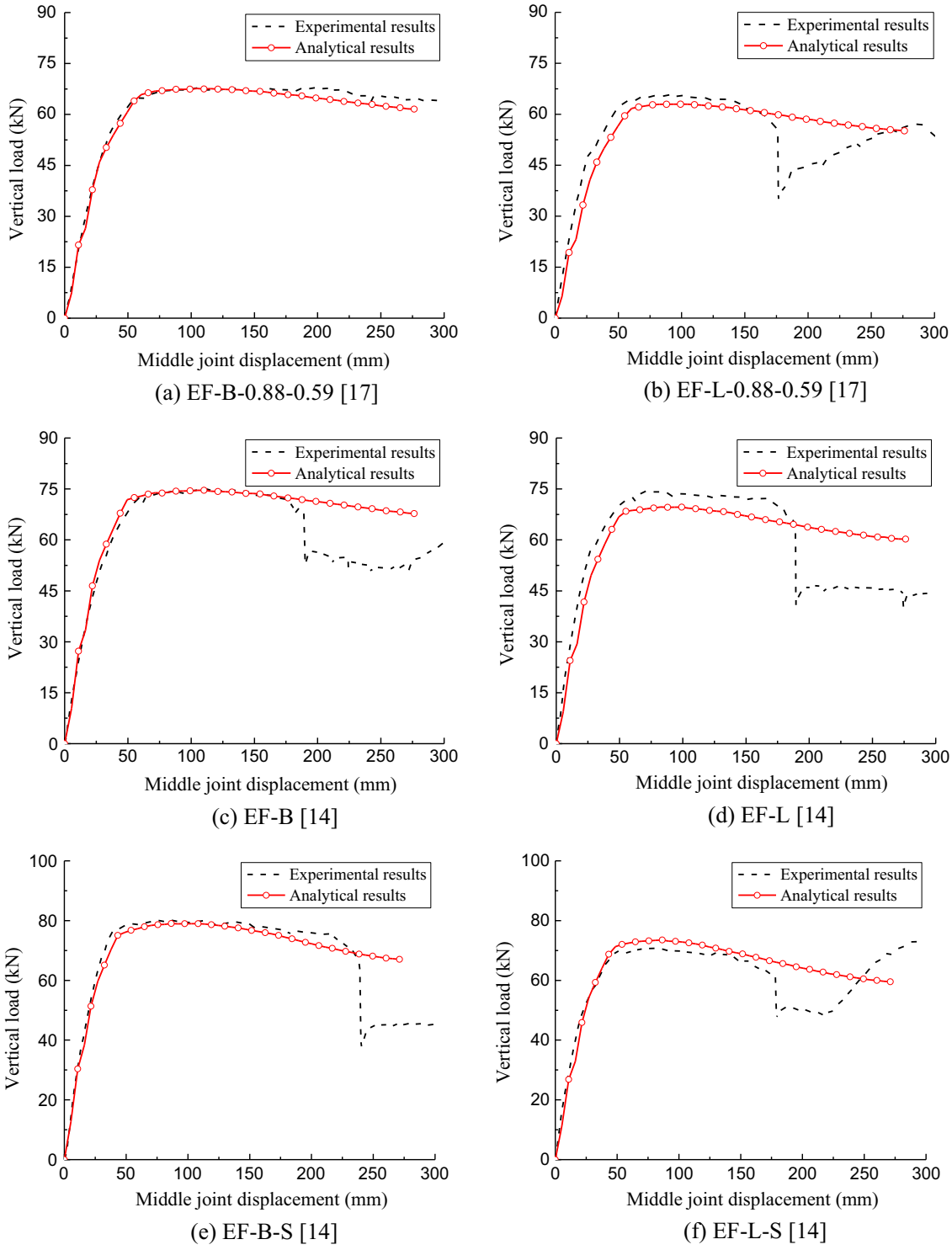

Fig. 7. Comparison between analytical and experimental vertical load-middle joint displacement curves (the vertical load and displacement can be calculated from Eqs. (5) and (2), respectively).

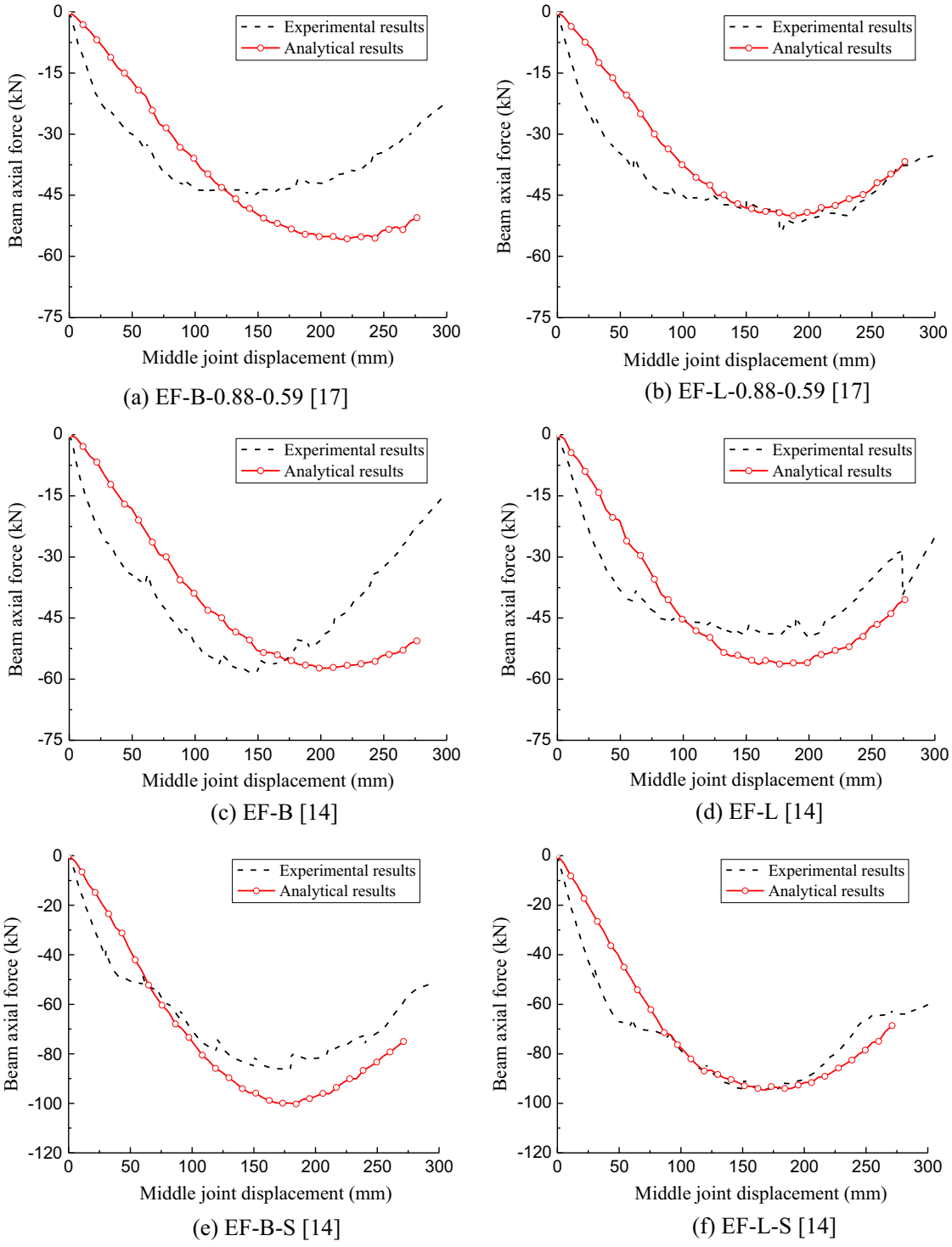

Fig. 8. Comparison between analytical and experimental beam axial force-middle joint displacement curves (the axial force and displacement can be calculated from Eqs. (6) and (2), respectively).

5.2. Effect on shear force and bending moment in the joint

Under CAA, net compression force in the beam increases the bending moment at the column-joint interface and shear force in the beam-column joint in comparison with that under flexural action. As a result, shear failure of reinforced concrete columns were observed in the experimental tests [14,16,25]. In this study, the effects of column height, column section and beam depth on the bending moment and shear force in the column are also evaluated in the analytical model.

Fig. 12 shows the equilibrium of a column subject to CAA. Horizontal forces T_{s1} and $C_{c1} + C_{s1}$ are obtained from the analytical model for CAA. It is assumed that compression force $C_{c1} + C_{s1}$ acts at the centroid of compressive reinforcement. Based on equilibrium of the column, reaction forces R_t and R_b at the top and bottom pin supports can be calculated from Eqs. (11) and (12).

Table 4
Comparisons between analytical and experimental results.

Specimen		Beam section (mm)	Rebar*	CAA (kN)			Beam axial compression (kN)		
				Analytical result P_a	Experimental result P_e	$\frac{P_a}{P_e}$	Analytical result N_a	Experimental result N_e	$\frac{N_a}{N_e}$
Kang and Tan [17]	EF-B-0.88-0.59	150 × 300	3T13 (top); 2T13 (bottom)	67.6	67.9	1.00	56.2	45.0	1.25
	EF-L-0.88-0.59			63.0	65.9	0.96	50.5	53.9	0.94
Kang and Tan [14]	EF-B		2T16 + T13 (top); 2T13 (bottom)	74.6	75.1	0.99	57.7	58.3	0.99
	EF-L			69.7	74.4	0.94	57.0	49.8	1.14
	EF-B-S			79.0	80.1	0.99	100.1	86.2	1.16
	EF-L-S			73.5	71.0	1.04	94.6	94.8	1.00
Yu [18]	F3-CA-NS-EX	150 × 250	3T13 (top); 2T13 (bottom)	46.1	45.9	1.00	40.9	48.9	0.84
	F4-CA-WS-EX			46.1	50.1	0.92	39.9	48.0	0.83
Sadek et al. [15]	IMF	711 × 508	4#8 (top); 2#9 (bottom)	286.9	296	0.97	1383.7	–	–
	SMF	864 × 660	7#8 (top); 6#8 (bottom)	933.2	900	1.04	3487.8	–	–
Mean value						0.99			1.02
Coefficient of variation						4%			15%

* T13 and T16 represent high yield-strength deformed bars with diameters of 13 mm and 16 mm, respectively. #8 and #9 denote steel reinforcement of 25.4 mm and 28.7 mm nominal diameters.

Table 5
Geometry and stiffness of reinforced concrete columns.

Parameter	Column section (mm)	Column height (mm)	Column Reinforcement	Beam section (mm)	Beam reinforcement	Lateral stiffness (kN/m)	Rotational stiffness (kN.m/rad)
Column height	300 × 300	1340	8T13	150 × 300	3T13 (top); 2T13 (bottom)	1.82×10^5	6.07×10^4
		2340				2.3×10^4	2.72×10^4
		3340				0.7×10^4	1.75×10^4
Column section	250 × 250	2340				1.2×10^4	1.36×10^4
	300 × 300					2.3×10^4	2.72×10^4
	350 × 350					4.0×10^4	4.97×10^4
	400 × 400					6.4×10^4	7.64×10^4
Beam depth	300 × 300			150 × 250		2.1×10^4	2.58×10^4
				150 × 300		2.3×10^4	2.72×10^4
				150 × 350		2.5×10^4	2.87×10^4
				150 × 400		2.7×10^4	3.04×10^4

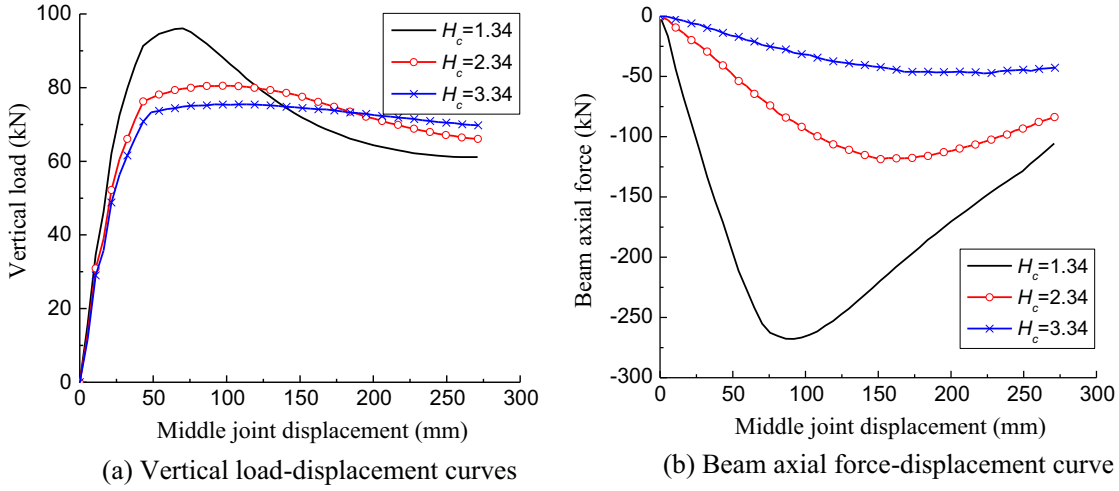

(a) Vertical load-displacement curves (b) Beam axial force-displacement curve

Fig. 9. Effect of column height on CAA and beam axial force.

$$R_t = \frac{(C_{s1} + C_{c1})(l_b + a'_{s1}) - T_{s1}(l_b + h - a_{s1})}{l_t + l_b + h} \quad (11)$$

$$R_b = \frac{(C_{s1} + C_{c1})(l_t + h - a'_{s1}) - T_{s1}(l_t + a_{s1})}{l_t + l_b + h} \quad (12)$$

where R_t and R_b are the reaction forces in the top and bottom lateral restraints, respectively; C_{s1} and C_{c1} are the compression forces sustained by steel reinforcement and concrete at Section 1; T_{s1} is the tension force sustained by reinforcement; l_b is the column length below the joint; and a'_{s1} is the distance between the centroid of compressive reinforcement and extreme compression concrete fibre at Section 1.

Under flexural action, axial compression force in the beam is zero and compression force $C_{s1} + C_{c1}$ sustained by compressive reinforcement and concrete is equal to tension force T_{s1} in tensile reinforcement. Accordingly, Eqs. (11) and (12) can be simplified as:

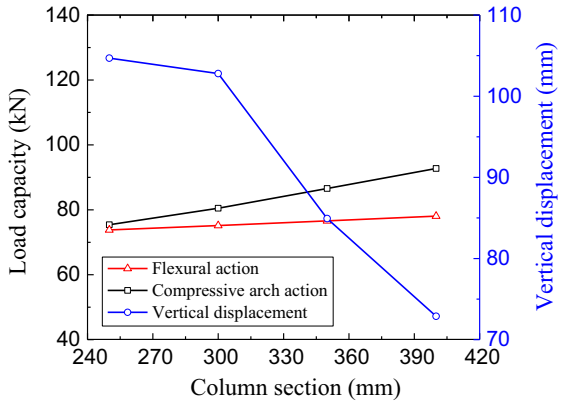

(a) CAA capacity and associated vertical displacement

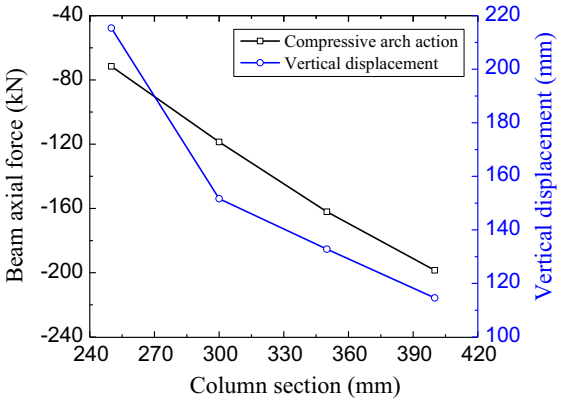

(b) Peak beam axial force and vertical displacement

Fig. 10. Effect of column cross section on CAA and beam axial force.

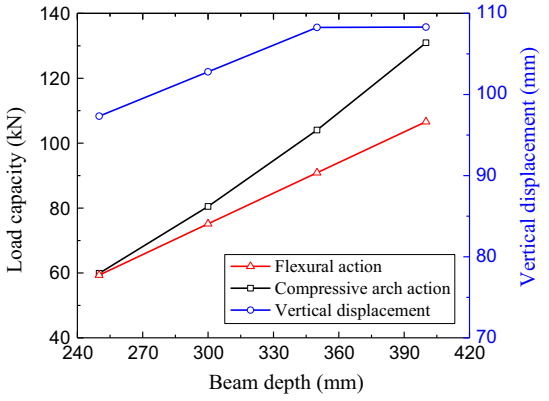

(a) CAA capacity and associated vertical displacement

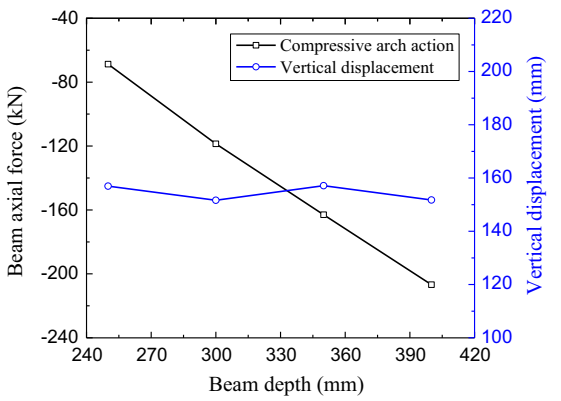

(b) Peak beam axial force and vertical displacement

Fig. 11. Effect of beam depth on CAA and beam axial force.

$$R_t = \frac{T_{s1}(a'_{s1} + a_{s1} - h)}{l_t + l_b + h} \tag{13}$$

$$R_b = \frac{T_{s1}(h - a'_{s1} - a_{s1})}{l_t + l_b + h} \tag{14}$$

Bending moment M_b at the joint face and shear force V_s in the joint can be determined from Eqs. (13) and (14), respectively.

$$M_b = R_b l_b \tag{15}$$

$$V_s = T_{s1} + R_t \tag{16}$$

where M_b is the bending moment at the column-joint interface and V_s is the shear force in the joint, as shown in Fig. 12.

Fig. 13(a) shows the effect of column height on the shear force in the beam-column joint. When the column height is 3.34 m, maximum shear force in the joint is 280.8 kN, only 12% greater than that under flexural action. By reducing its height from 3.34 m to 1.34 m, the shear force is considerably increased to 358.4 kN, about 56% greater than the value generated by flexural action. In the meantime, corresponding vertical displacement is reduced from 222.4 mm to 98.3 mm. On the contrary, if flexural action is considered, shear force in the joint is reduced from 258.4 kN to 230.0 kN when the column is shortened from 3.34 m to 1.34 m, as included in Table 6. Hence, CAA in the beam significantly increases shear force in the joint, in particular when the column height is comparatively short. If shear reinforcement in the joint is designed in accordance with the shear force under flexural action, shear failure of the joint may occur when CAA develops in the connecting beam.

Besides shear force in the beam-column joint, bending moment at the joint face is also calculated in the model. Fig. 13(b) shows the variations of bending moment with various column heights. By reducing the column height from 3.34 m to 1.34 m, bending moment at the joint face is increased from 68.8 kN.m to 105.9 kN.m, even though the distance between the bottom pin support and joint is reduced. The increase in bending moment results from the increased axial compression force in the beam. Comparisons are also made between the calculated bending moment and the moment capacity of the column. Under an axial load ratio of 0.3, the moment capacity of the column is calculated as 118.9 kN.m (see Table 6), around 12% greater than the maximum bending moment of the 1.34 m high column subject to CAA. Therefore, for the range of column heights in the study, flexural failure of the column will not occur.

It is well known from statics that shear force in the joint and bending moment at the column-joint interface do not vary with column section, as shown in Table 6. However, when CAA is taken into consideration, increasing the cross section of column will also lead to an increase in the joint shear force, as shown in Fig. 14(a).

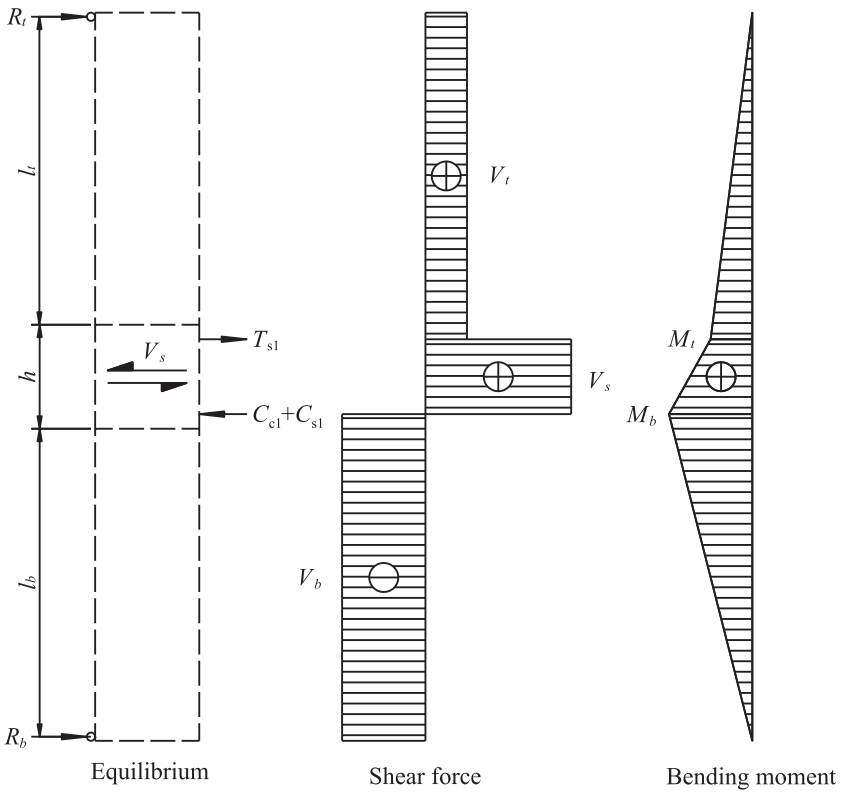

Fig. 12. Equilibrium of reinforced concrete column.

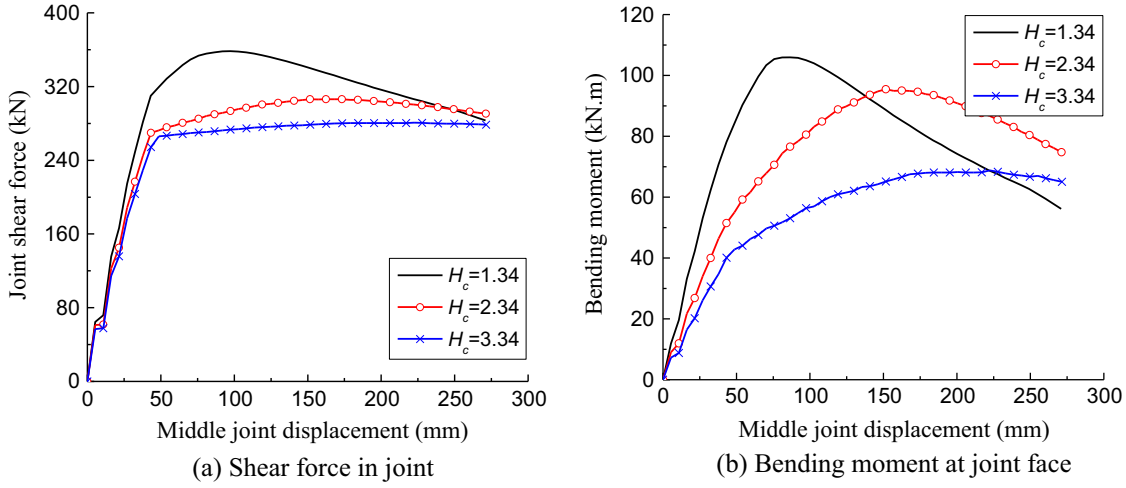

Fig. 13. Effect of column height on shear force and bending moment in column.

For instance, by enlarging the cross section from 250 mm to 400 mm, the maximum shear force is almost linearly increased by roughly 22% from 283.7 kN to 345.9 kN and associated vertical displacement is reduced from 209.8 mm to 127.4 mm. As the column section is enlarged, average shear stress in the joint needs to be examined to estimate the potential failure mode of the joint. Table 6 shows the average shear stress in the beam-column joint, calculated as the joint shear force divided by the cross sectional area of the column. It turns out that when the column section is 250 mm, shear force in the joint is 4.5 MPa, close to the stress limit specified by ACI [23], i.e., $1.0\sqrt{f'_c}$. It indicates that shear failure is likely to occur when the column section is small. Joint shear stress is reduced by increasing the column section, even though shear force is increased. Thus, shear failure of the joint can be prevented in columns with relatively greater cross section. Furthermore, bending moment at the joint face is increased by 71% from 69.6 kN.m to 134.7 kN.m when the column section is increased from 250 mm to 400 mm (see Fig. 14(b)). Nevertheless, moment capacity of the column is also increased by 121% from 77.8 kN.m to 238.4 kN.m, as included in Table 6. Therefore, flexural failure of the column will not take place by enlarging the column section.

Fig. 15 shows the effect of beam depth on the shear force and bending moment in the joint. Under flexural action, shear force in the joint decreases as the beam depth increases. On the contrary, as a result of the development of CAA, shear force in the joint is increased from 288.8 kN to 336.1 kN, as shown in Fig. 15(a), when

Table 6
Shear force and bending moment in column.

Parameter	Column section (mm)	Column height (mm)	Beam section (mm)	Shear force in the joint (kN)		Shear stress under CAA (MPa)	Bending moment at joint face (kN.m)		Moment capacity (kN.m)
				Flexural action	CAA		Flexural action	CAA	
Column height	300 × 300	1340	150 × 300	230.0	358.4	4.0	26.8	105.9	118.9
		2340		250.3	306.2	3.4	28.9	95.5	
		3340		258.4	280.8	3.1	29.8	68.8	
Column section	250 × 250	2340		250.3	283.7	4.5	28.9	69.6	77.8
	300 × 300				306.2	3.4		95.5	118.9
	350 × 350				328.2	2.7		118.9	171.8
	400 × 400				346.3	2.2		138.2	238.4
Beam depth	300 × 300		150 × 250	256.2	288.8	3.2	23.1	62.1	118.9
			150 × 300	250.3	306.2	3.4	28.9	95.5	
			150 × 350	244.3	321.4	3.6	34.4	123.9	
			150 × 400	238.4	336.1	3.7	39.6	151.1	

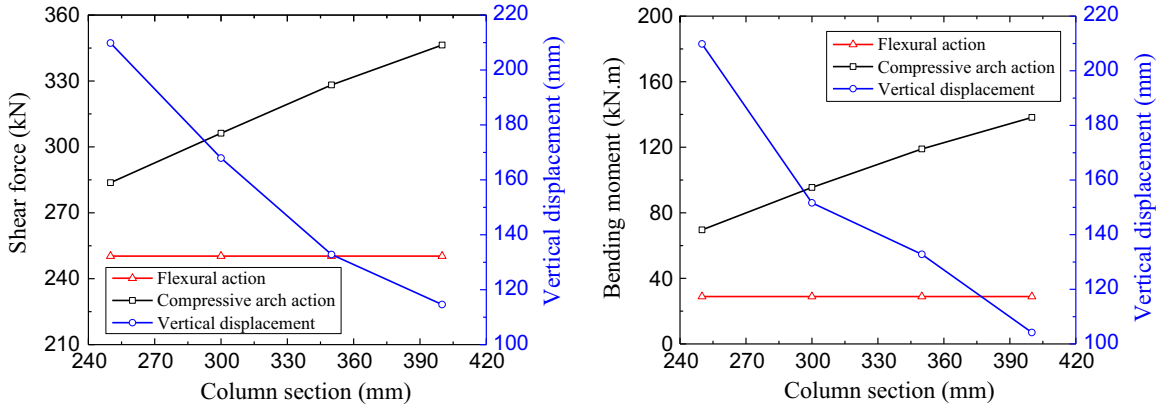

(a) Maximum shear force in joint and associated displacement

(b) Maximum bending moment at joint face and associated displacement

Fig. 14. Effect of column cross section on shear force and bending moment in column.

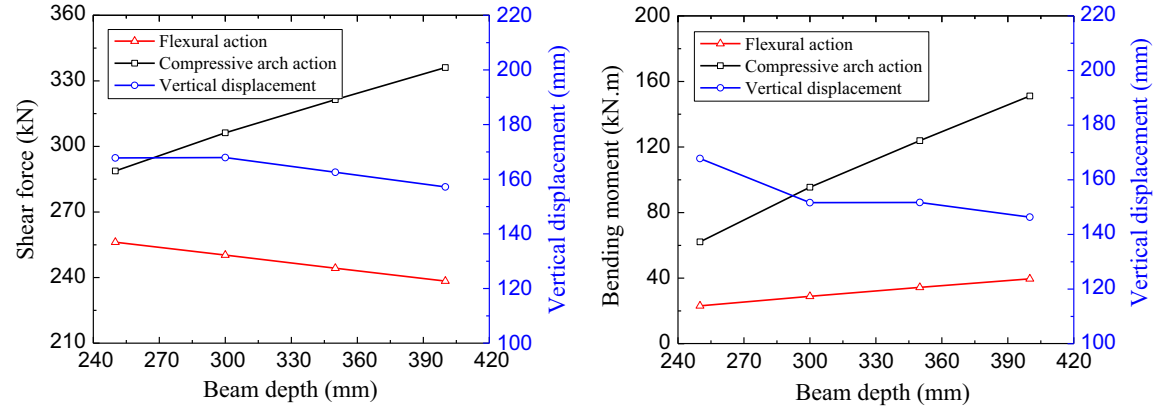

(a) Maximum shear force in joint and associated displacement

(b) Maximum bending moment at joint face and associated displacement

Fig. 15. Effect of beam depth on shear force and bending moment in column.

the beam depth is increased from 250 mm to 400 mm. There are minor differences between corresponding vertical displacements. Besides, the difference between joint shear forces under flexural action and CAA becomes increasingly greater, as shown in Table 6. Nearly the same effect is observed on the bending moment at the joint face and associated vertical displacement (see Fig. 15(b)). By increasing the beam depth from 250 mm to 400 mm, bending moment at the joint face is increased by 129% from 62.1 kN.m to 151.1 kN.m. Comparison between the calculated bending moment and the moment capacity of column section shows that flexural failure of the column will occur when the beam depth is increased to 400 mm.

Parametric studies on the effects of column height, column cross section and beam depth suggest that relatively short reinforced concrete columns with small cross section are favourable to the development of significant CAA in the connecting beam with

greater depth. However, flexural or shear failure of columns may occur as a result of increased shear force in the joint and bending moment at the joint face. Therefore, additional shear force and bending moment generated by CAA in the beam have to be considered in the design of columns and beam-column joints.

6. Conclusions

In this paper, an analytical model for CAA in reinforced concrete frames is introduced, in which flexural and rotational stiffness of columns is taken into consideration. Besides, similar rigid-plastic assumption is used for quantifying the stiffness of columns. The analytical model is validated against experimental results and reasonably good accuracy is obtained in terms of the load capacity and axial compression force in the beam. Moreover, parametric studies are carried out to investigate the effects of column height, column section and beam depth on the CAA of beams. Focus is placed on the shear force in the beam-column joint and bending moment at the joint face, as they are increased by the CAA in the beam. The following conclusions can be drawn from the analytical studies.

(1) Increases in horizontal and rotational stiffness of side columns, such as reducing the column height, enlarging the column section or increasing the beam depth, result in increases in the CAA capacity and beam axial compression force. Therefore, relatively stiff column and deep beam are preferred to mobilise significant CAA in the beam.
(2) Compared to flexural action, shear force in the side beam-column joint and bending moment at the joint face are considerably increased with the development of significant CAA in the beam. As a result, shear or flexural failure of the column is likely to occur, in particularly when the column height is comparatively short, the column section is small and the beam depth is great.

Generally, development of CAA increases the resistance of the beam if adequate lateral and rotational restraints are provided for the beam. However, it may lead to premature shear or flexural failure of the connecting column due to the presence of axial compression force in the beam. Thus, in the design of columns, special attention has to be paid to the flexural and shear resistances when CAA develops in the adjacent beams.

Acknowledgements

The authors gratefully acknowledge the financial support provided by the National Natural Science Foundation of China (No. 51608068), Fundamental and Frontier Research Project of Chongqing (No. cstc2016jcyjA0450) and China Postdoctoral Science Foundation (2016M590863).

References

[1] Park R. The ultimate strength and long-term behaviour of uniformly loaded, two-way concrete slabs with partial lateral restraint at all edges. Mag Concr Res 1964;16:139–52.
[2] Welch RW, Hall WJ, Gamble WL. Compressive membrane capacity estimates in laterally edge restrained reinforced concrete one-way slabs. UILU-ENG-99-2009. Department of Civil and Environmental Engineering, University of Illinois at Urbana-Champaign; 1999.
[3] Park R, Gamble WL. Reinforced concrete slabs. John Wiley & Sons, Inc; 2000.
[4] Guice LK, Slawson TR, Rhomberg EJ. Membrane analysis of flat plate slabs. ACI Struct J 1989;86:83–92.
[5] Yu J, Tan KH. Analytical model for the capacity of compressive arch action of reinforced concrete beam-column sub-assemblages. Mag Concr Res 2013;66:109–26.
[6] Kang S-B, Tan KH. Analytical model for compressive arch action in horizontally-restrained beam-column sub-assemblages. ACI Struct J 2016;113:813–26.
[7] Izzudin BA, Vlassis AG, Elghazouli AY, Nethercot DA. Progressive collapse of multi-storey buildings due to sudden column loss – Part I: simplified assessment framework. Eng Struct 2008;30:1308–18.
[8] FarhangVesali N, Valipour H, Samali B, Foster S. Development of arching action in longitudinally-restrained reinforced concrete beams. Constr Build Mater 2013;47:7–19.
[9] Su Y, Tian Y, Song X. Progressive collapse resistance of axially-restrained frame beams. ACI Struct J 2009;106:600–7.
[10] Kang S-B, Tan KH. Behaviour of precast concrete beam-column sub-assemblages subject to column removal. Eng Struct 2015;93:85–96.
[11] Kang S-B, Tan KH, Yang E-H. Progressive collapse resistance of precast beam-column sub-assemblages with engineered cementitious composites. Eng Struct 2015;98:186–200.
[12] Yu J, Tan KH. Experimental and numerical investigation on progressive collapse resistance of reinforced concrete beam column sub-assemblages. Eng Struct 2013;55:90–106.
[13] Yu J, Tan KH. Structural behavior of RC beam-column subassemblages under a middle column removal scenario. J Struct Eng 2013;139:233–50.
[14] Kang S-B, Tan KH. Robustness assessment of exterior precast concrete frames under column removal scenarios. J Struct Eng 2016;142:04016131.
[15] Sadek F, Main JA, Lew HS, Bao Y. Testing and analysis of steel and concrete beam-column assemblies under a column removal scenario. J Struct Eng 2011;137:881–92.
[16] Choi H, Kim J. Progressive collapse-resisting capacity of RC beam-column sub-assemblage. Mag Concr Res 2011;63:297–310.
[17] Kang S-B, Tan KH. Progressive collapse resistance of precast concrete frames with discontinuous reinforcement in the joint. J Struct Eng 2017.
[18] Yu J. Structural behaviour of reinforced concrete frames subjected to progressive collapse. Singapore: Nanyang Technological University; 2012.
[19] Keenan WA. Strength and behavior of restrained reinforced concrete slabs under static and dynamic loading. Technical Report R-621. Port Hueneme, CA: Naval Civil Engineering Laboratory; 1969.
[20] Mander JB, Priestley MJN, Park R. Theoretical stress-strain model for confined concrete. J Struct Eng 1988;114:1804–26.
[21] Soesianawati MT. Limited ductility design of reinforced concrete columns. New Zealand: University of Canterbury; 1986.
[22] Watson S, Park R. Simulated seismic load tests on reinforced concrete columns. J Struct Eng 1994;120:1825–49.
[23] ACI. Building code requirements for structural concrete. ACI 318-11. Farmington, MI: American Concrete Institute; 2011.
[24] Paulay T, Priestley MJN. Seismic design of reinforced concrete and masonry buildings. John Wiley & Sons; 1992.
[25] Lew HS, Bao Y, Sadek F, Main JA, Pujol S, Sozen MA. An experimental and computational study of reinforced concrete assemblies under a column removal scenario. NIST Technical Note 1720. Gaithersburg, MD: National Institute of Standards and Technology; 2011.